Chapter 1. Introduction

1.1 Preface

Nanotechnology, one of the leading trends in the 21st century, which meets the future needs for miniaturization of devices into nanometer while their ultimate performance is significantly improved. For its fascinating and peculiar properties, this raises many issues by making new types of nanostructures or simply by down-sizing existing microstructures into the 1-100 nm regime.

Since the first observation of carbon nanotube (CNT) [1], its astounding properties [2] which include ballistic electron transport, high mechanical strength and flexibility, are of great interest to the scientific and industrial communities. Figure 1.1 shows structure and morphology of CNTs, which we can clearly see that nanotubes formed by ropes of graphite layer. In addition to their fundamental scientific importance, CNT has numerous potential applications in nanoelectronics [3], nanoscale structural materials, hydrogen storage [4,5] and field emission devices [6,7] among others.

Carbon nanotubes have emerged as one of the most promising electron field emitters since 1998 [8]. The power of CNTs as electron sources for displays and lighting devices was demonstrated in the last few years. Lighting elements based on CNT cathodes have been presented in 1998 and are commercially available with lifetimes in excess of 8000 hours [9,10]. Samsung has already developed a sealed full-color 9” display few years ago [7,11]. This display representes an impressive feat and an important milestone towards a fully functional device.

Ever since the development of carbon nanotube-based display, great efforts were invested in the performance improvement of field emission display (FED). We consider it an attractive alternative to liquid crystal display (LCD).

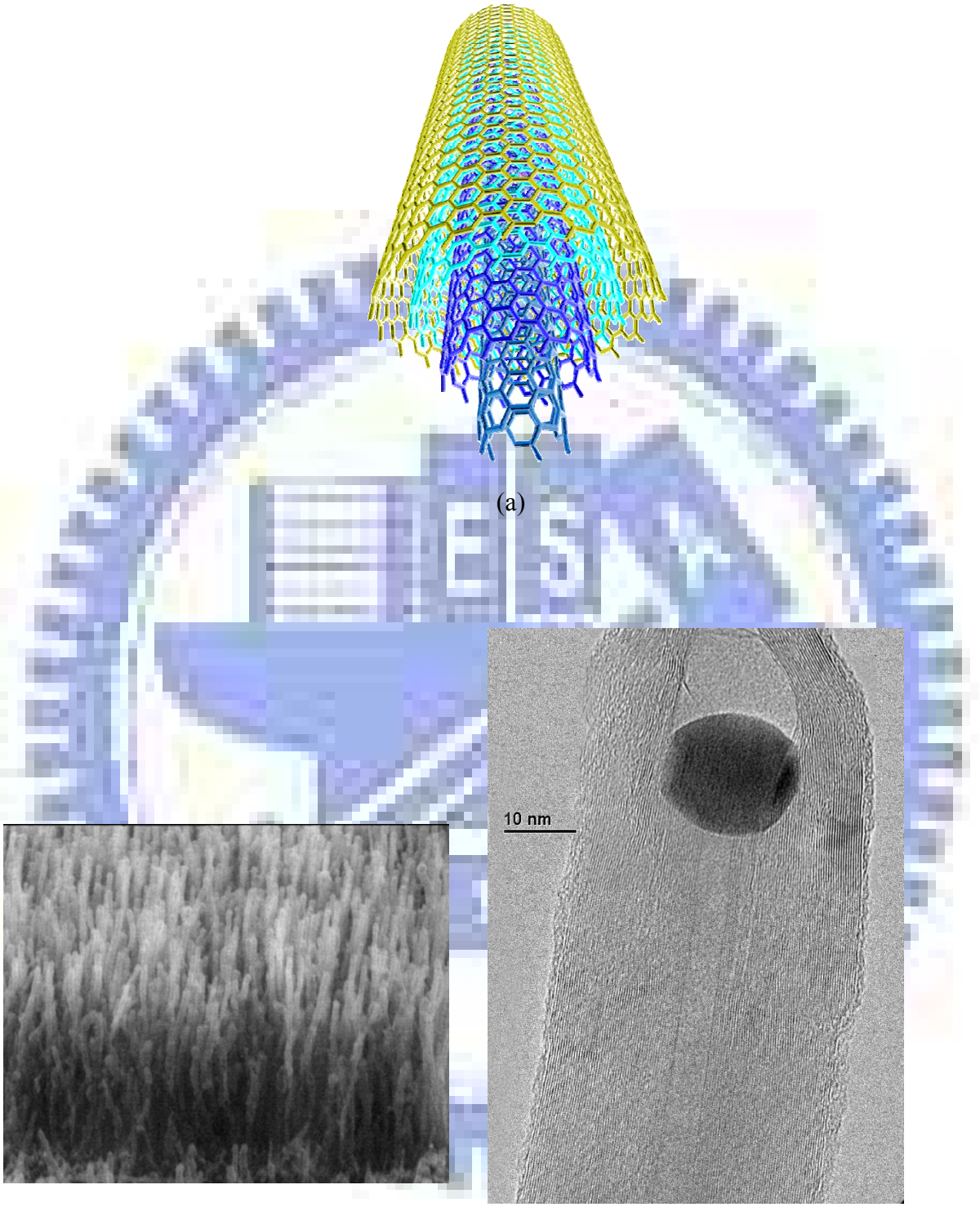

(a)

(b) (c)

Fig. 1.1 Images of carbon nanotube (CNT) : (a) simulated atomic structure (b) SEM image (c) TEM image

1.2 Literature Review of Density-Controlled Carbon Nanotubes Growth Methods with Chemical Vapor Deposition System

Until now, the most critical factor for growing density-controlled carbon nanotubes with CVD system is controlling the distribution and density of catalyst. The catalyst are commonly transition metal especially Fe, Ni and Co.

1.2.1 Catalyst controlled with pulse-current electrochemical deposition

Y. Tu. and his group used the pulse-current electrochemical deposition to control catalyst density [12]. Previously, electrochemical deposition was used to synthesize metal nanoparticles with high density, small size, and uniform diameter such as Ni, Ag, Au, Pt nanoparticles for applications in catalysis, electronics, and sensors. In Tu's article, the nucleation site density and the size of nickel nanoparticles were controlled in a wide range from 10^5 to 10^8 cm^{-2} by adjusting the amplitude of the pulse current, duration and electrolyte concentration. Figure 1.2 shows the density controlled CNTs prepared by Tu et. al.

1.2.2 Catalyst controlled by reducing the deposition yield through catalyst interaction with interface diffusion layer

K.B.K. Teo. and his group demonstrated a method to reduce the site of nickel nanoparticles with interface diffusion layer between nickel and silicon layers [13]. They claimed that nickel would clearly remain on the surface of titanium nitride (TiN) which acted as a good barrier against diffusion of Ni into Si. In contrast to tungsten nitride (WN) which served as imperfect diffusion barrier would result in leaving small amount of nickel on the surface of WN. Figure 1.3 shows the density controlled CNTs in Teo's article.

1.2.3 Catalyst controlled by electron beam lithography technique

Electron beam lithography is the most common method to control the distribution and density of catalyst [13~15]. But it is still the method that needs the most semiconductor procedures resulting in high expense. The quality of density-controlled CNTs grown by lithography deposited catalyst seem to be excellent without any other carbide by-products. Figure 1.4 shows the patterned CNTs grown with e-beam lithography technique.

1.3 Review of Field Emission Display Technology

Display devices play a very important role in today's information-dominated society. The research of field emission started in 1928 when Fowler-Nordheim theory was proposed [16]. Later, C.A. Spindt invented the field emitter arrays (FEAs) [17,18], which are fabricated via evaporation of the materials through shrinking aperture. Field emission displays (FEDs) are similar to cathode ray tubes (CRTs) in the sense that the display image results from cathodoluminescence of phosphor materials. In FEDs, multiple electron beams are generated from the field emission cathode and no scanning of beams is required [19]. Figure 1.5 represents a simplified cross section of a FED panel. The anode voltage is limited by breakdown around spacers. FEDs comparing to LCDs offer many advantages as following :

Viewing angle

As a display, it should meet the basic need for letting users see the exact images. LCDs, nowadays, still remain difficult for users to read at modest off-axis angles. No mention the angle near 90°off-axis angle. FEDs are emissive which allow equal brightness and contrast at all angle.

Brightness

Outdoor instruments require high brightness to compete with direct sunlight. So

reflective displays such as LCDs are difficult to read outdoor or in the case users being far from the displays FEDs are emissive displays that produce their own light, they can be dimmed continuously from full brightness to less than 0.05 fL.

Speed

Display speed is the rate at which the image can be changed while maintaining image detail. Displays with inadequate response times will create image "smear" that can be confused with defective blood flow, or will hide jitter that can indicate instability or electrical interference. With a response time of 20 nanoseconds, FED technology produces smear-free video images.

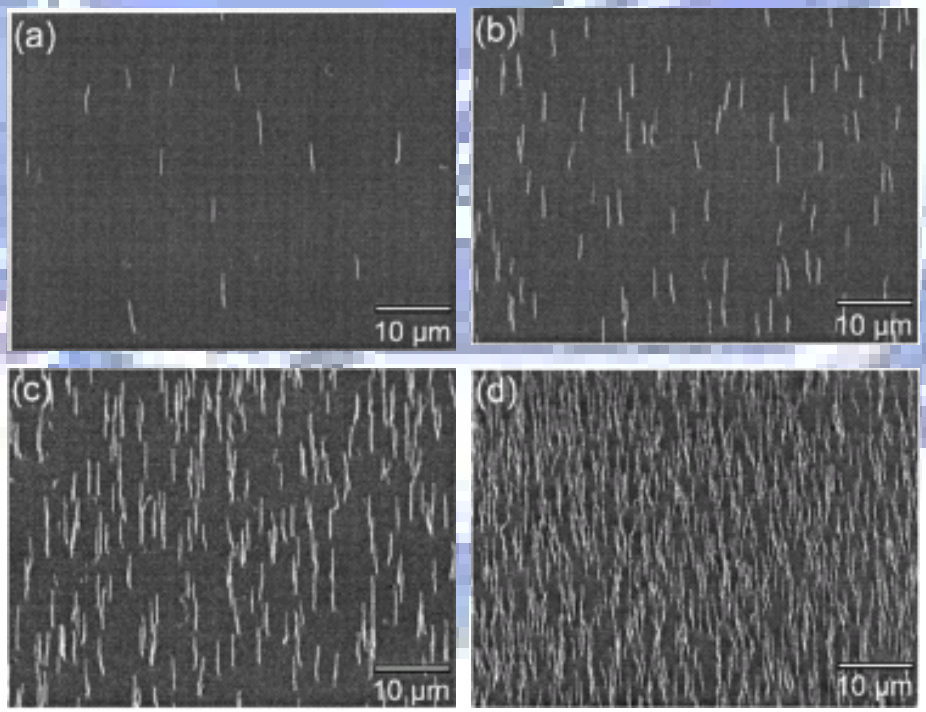

Fig. 1.2 SEM imges of CNTs with site density of (a) $7.5x10^5$ cm^{-2} (b) $2x10^6$ cm^{-2} (c) $6x10^6$ cm^{-2} (d) $2x10^7$ cm^{-2}

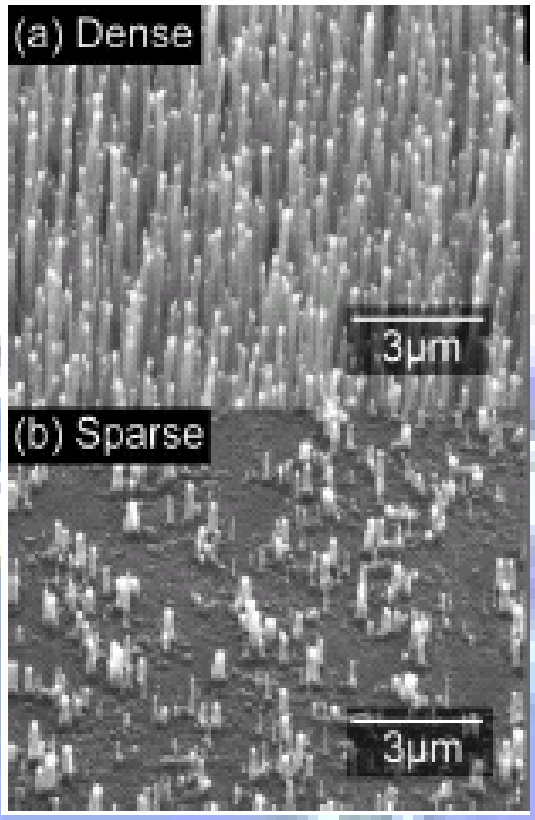

Fig. 1.3 (a) Densely packed of CNTs (b) Sparse packed of CNTs

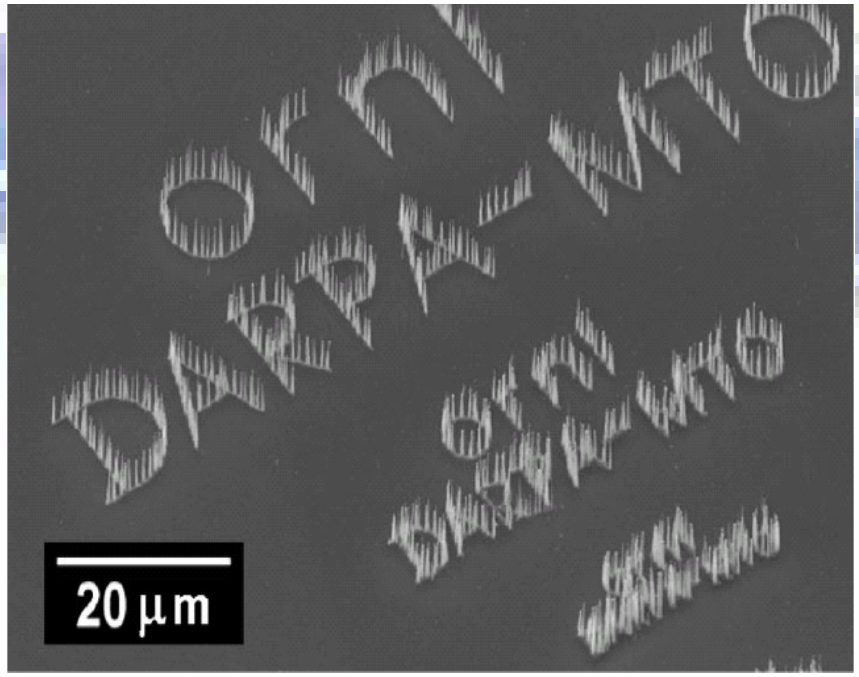

Fig. 1.4 SEM image of patterned growth CNTs

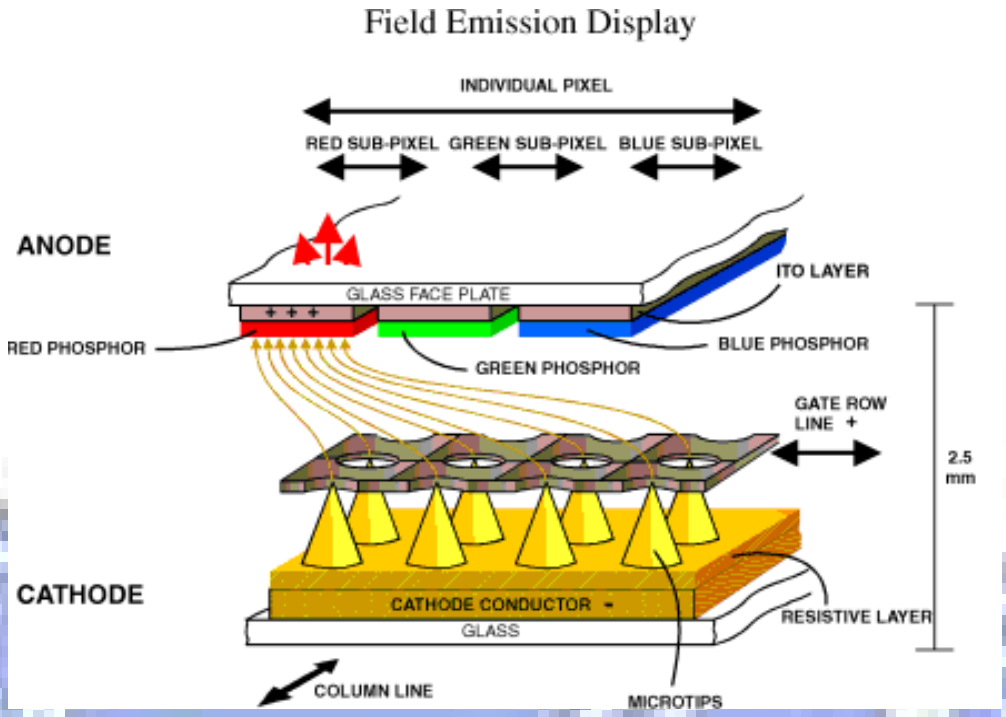

Fig. 1.5 Schematic diagram of a field emission cell

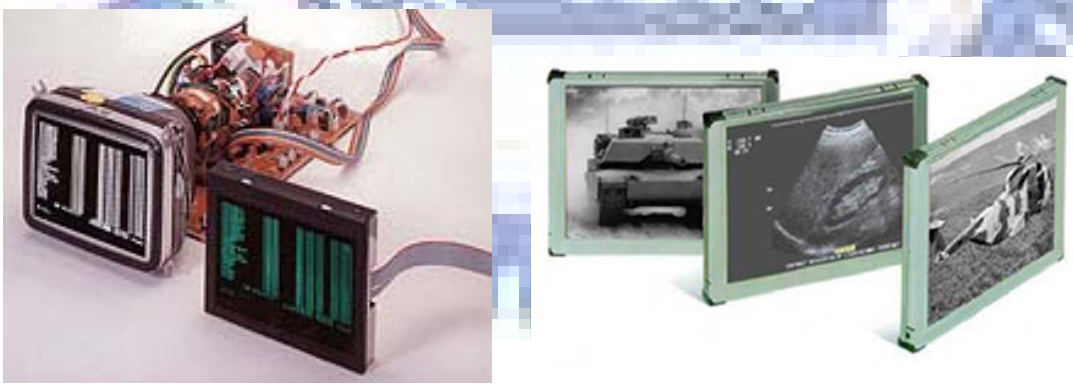

(a) **(b)**

Fig. 1.6 (a) Comparison between traditional CRT (left) and FED (right), and (b) products of FED

1.4 Motivation

L. Nilsson's group [16] had shown experimentally and theorectically that the density of the nanotubes plays a crucial role for the field emission properties. The CNT films of low density yield low current essentially because the emitter density and the β factor are low. For high density films, screening effects reduce the field enhancement and thus the emitted current. For films of medium density, there is an ideal compromise between the emitter density and the intertube distance, which is sufficiently large to avoid screening effects. Their calculations predict that an intertube distance of about 2 times the height of the CNTs optimizes the emitted current per unit area. Subsequently, other groups [17,18] also verify the screening effects in field emission and predict that if the ratio of intertube distance to tube height is around 1～2, the emitted current will be optimized.

The methods previously proposed for controlling density of CNT remain challenges to deal with. First, it is still lack of method to exactly control density, even the distribution of CNTs. Second, in use of e-beam lithography may result in higher cost. In this thesis, we attempt to establish a new method to grow density-controlled CNTs. Simultaneously, we compare the field emission property of CNTs with different density in consideration to screening effects.

Chapter 2. Fundamental Theories

2.1 Theory of Field Emission

2.1.1 Field Emission from Metals

Field emission is a quantum-mechanical phenomenon in which electrons tunnel through a potential barrier at the surface of a solid as a result of the application of a large electric field. Field emission is distinct from thermionic emission and photoemission in which electrons acquire sufficient energy *via* heating or energy exchange with photons, respectively, to overcome (go over) the potential barrier. In field emission, external electric field at the order of 10^7 V cm^{-1} is required for appreciable electron currents. The presence of the electric field reduces the width of the potential barrier and therefore is permeable to the electrons. This can be seen with the aid of Fig. 2.1 which presents a diagram of the electron potential energy at the surface of a metal.

The dashed line in Figure 2.1 shows the shape of the barrier in the absence of an external electric field. The height of the barrier is equal to the work function of the metal, φ, which is defined as the energy required removing an electron from the Fermi level E_F of the metal to a rest position just outside the material (the vacuum level). The solid line in Figure 2.1 corresponds to the shape of the barrier in the presence of the external electric field. As can be seen, in addition to the barrier becoming triangular in shape, the height of the barrier in the presence of the electric field E is smaller, with the lowering given by [20]

$$\Delta\phi = \left(\frac{eE}{4\pi\varepsilon_0} \right)^{1/2} \tag{2.1}$$

where e is the elementary charge and ε_0 is the permittivity of vacuum.

Knowing the shape of the energy barrier, one can calculate the probability of an electron with a given energy tunneling through the barrier. Integrating the probability function multiplied by an electron supply function in the available range of electron energies leads to an expression for the tunneling current density J as a function of the external electric field E. The tunneling current density is expressed by Eq. (2.2) which is known as the Fowler-Nordheim equation [21][22]

$$J = \frac{e^3 E^2}{8\pi h \phi t^2(y)} \exp\left[\frac{-8\pi(2m)^{1/2}\phi^{3/2}}{3heE} v(y)\right] \qquad (2.2)$$

where $y = \Delta\varphi/\varphi$ with $\Delta\varphi$ given by Eq. (2.1), h is the Planck's constant, m is the electron mass, and $t(y)$ and $v(y)$ are the Nordheim elliptic functions; to the first approximation $t^2(y) = 1.1$ and $v(y) = 0.95 - y^2$. Substituting these approximations in Eq. (2.2), together with Eq. (2.1) for y and values for the fundamental constants, one obtains

$$J = 1.42\times10^{-6}\frac{E^2}{\phi}\exp\left(\frac{10.4}{\phi^{1/2}}\right)\exp\left(\frac{-6.44\times10^7\phi^{3/2}}{E}\right) \qquad (2.3)$$

where J is in units of A cm^{-2}, E is in units of V cm^{-1} and φ in units of eV. Plotting $\log(J/E^2)$ *vs.* $1/E$ results in a straight line with the slope proportional to the work function value, φ, to the 3/2 power. Equation (2.3) applies strictly to environment at temperature equal to 0^{o}K. However, it can be shown that the error involved in the use of the equation for moderate temperatures (300^{o}K) is negligible [23].

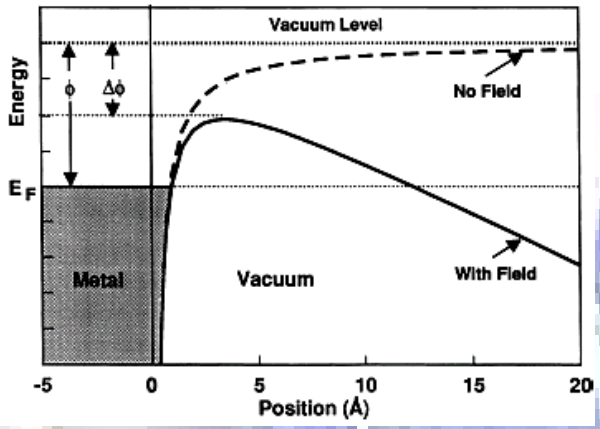

Fig. 2.1 Diagram of potential energy of electrons at the surface of a metal.

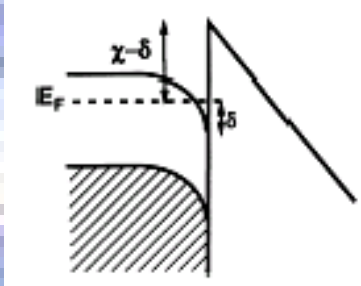

Fig. 2.2 Diagram of the potential energy of electrons at the surface of an n-type semiconductor with field penetration into the semiconductor interior.

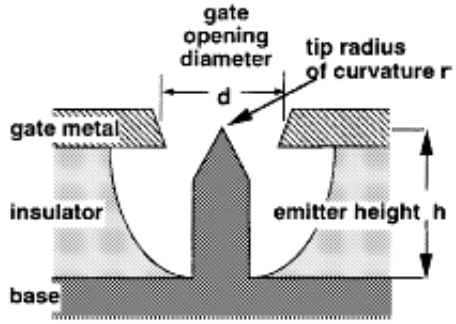

Fig. 2.3 Schematic diagram of a cell in a FEA. The emitter height is denoted by h, the gate aperture diameter by d, and the tip curvature by r.

2.1.2 Field Emission From Semiconductors

To a large degree, the theory for electron emission from semiconductors can be derived parallel to the theory for metals. However, special effects are associated with semiconductors due to the state of their surface and the fact that an external field applied to a semiconductor may penetrate to a significant distance into the interior. The classic theoretical treatment of electron emission from semiconductors is given in Ref. [24]. For the case when the external electric field penetrates into the interior of an *n*-type semiconductor and the surface states are neglected, $\log(J/E^2)$ is shown to be a linear function of $1/E$. However, in place of the work function φ in the Fowler-Nordheim equation one needs to substitute a quantity χ-δ, where χ is

the electron affinity defined as the energy required for removing an electron from the bottom of the conduction band of the semiconductor to a rest position in the vacuum, and δ denotes the band bending below the Fermi level. These parameters are illustrated in Fig. 2.2. The linear dependence of $\log(J/E^2)$ on $1/E$ is expected only if the density of the current flowing through the sample is much smaller than the current limiting density $J_{lim} = en\mu_n E/\varepsilon$, where μ_n is the electron mobility and n is the electron concentration in the bulk of the semiconductor [25][26]. At $J \approx J_{lim}$, the Fowler-Nordheim character of the relationship $J(E)$ passes into the Ohm's law (if the dependence of electron mobility on the electric field is neglected) which results in the appearance of the saturation region in the emission current vs. voltage curve [27]. Such saturation regions were observed experimentally for lightly doped *n*-type semiconductors and for *p*-type semiconductors [28][29]. Electron emission from semiconductors has been a subject of more recent theoretical considerations which takes into account complications due to electron scattering, surface state density, temperature, and tip curvature[30][31][32].

2.1.3 Fowler-Nordheim equation for a single-cell gated FEA

Figure 2.3 presents a schematic diagram of a cell in a microfabricated gated FEA. The emitter has the form of a sharp tip so that advantage can be taken of the well-known enhancement of electric field at surfaces exhibiting high curvature. If voltage V_g is applied to the gate electrode, the electric field E at the tip is given by Eq. (2.4)

$$E = \beta \times V \tag{2.4}$$

where the proportionality constant β is called the field enhancement or field conversion

factor. If E is in units of V cm^{-1} and V_g is in units of V, β is in units of cm^{-1}. If the area from which emission of electrons takes place is denoted as α, and Eq. (2.4) is substituted for E in the Fowler-Nordheim equation Eq. (2.3), the following expression is obtained

$$I = J \times \alpha = A \times V_g^2 \exp\left(-B / V_g\right) \tag{2.5}$$

where

$$A = 1.42 \times 10^{-6} \times \alpha \times \beta^2 / \phi \times \exp\left(10.4 / \phi^{1/2}\right) \tag{2.6}$$

and

$$B = 6.44 \times 10^7 \times \phi^{3/2} / \beta \tag{2.7}$$

In Eq. (2.5) I is in units of A, α in units of cm^2, β in units of cm^{-1}, φ in units of eV and V_g in units of V.

Plotting experimental values of electron emission current *vs*. gate voltage in the so-called Fowler-Nordheim coordinates, $log(I/V_g^2)$ *vs.* $1/V_g$, is a common way of analyzing electrical performance data for gated field emitter arrays. As can be seen from Eq. (2.5), such a plot will appear as a straight line over a large portion of the emission region. The constants A and B in Eq. (2.5) provide a way of comparing performance of FEAs with different geometrical parameters, emitter materials, *etc*. over a wide range of emission currents. The A and B values can be extracted from the least-squares fit to experimental data with A related to the intercept and B to the slope of the straight line in the Fowler-Nordheim coordinates.

2.1.4 Field enhancement and work function effects

Electron emission current is a strong function of the field enhancement β and work function ϕ. As an example, Fig. 2.4 (a) shows plots of emission current J, calculated using Eq. (2.5), as a function of gate voltage V_g for the fixed value of ϕ = 4eV and β varying from 3 x 10^5 to 6 x 10^5 cm^{-1}. Fig. 2.4 (b) shows plots of J vs. V_g for the fixed value of β = 4 x 10^5 cm^{-1} and ϕ varying from 2 to 5 eV.

The plots show that increasing β for lowering ϕ causes significant increase in the emission current density for a given gate voltage. For example, increasing β by 25% from 4 x 10^5 to 5 x 10^5 cm^{-1} at the gate voltage of 100V (Fig. 2.4 (a)) results in an order of magnitude increase of the emission current density, namely, from about 2 x 10^5 to 4 x 10^6 A/cm^2. An even stronger effect is observed for decreasing the work function value. For the gate voltage of 100V, decreasing the work function ϕ from 4 to 3 eV (Fig. 2.4 (b)) results in more than two orders of magnitude increase of the emission current density, i.e. from 2 x 10^5 to over 1 x 10^8 A/cm^2.

To analysis the effects of device geometry on the device performance, electric field values at the emitter tip can be calculated as functions of these parameters, using finite-element field calculation methods. It has shown [33-36] that the tip radius of curvature and the gate aperture diameter influence β most significantly; *i.e.* β increases rapidly as r and d decrease. A less significant effect is produced by the tip height h [37] and the tip position c [34], relatively to the center of the gate metal layer thickness. In particular, centering the tip vertically in the gate metal, corresponding to c = 0, produces the highest value of β.

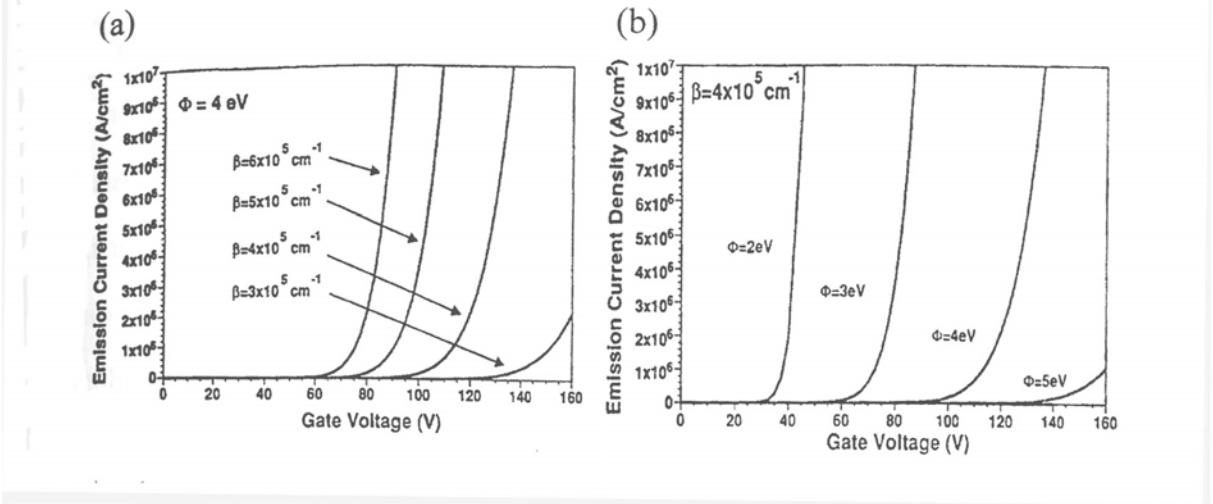

Fig. 2.4 Emission current density as a function of gate voltage for :

(a) the fixed of ϕ=4 eV and varying values of β

(b) the fixed value of β=4 x 10^5 cm^{-1} and varying values of ϕ

2.2 Growth Mechanisms

Growth mechanism of various kind of bottom-up nano size materials are generally considered to be three model: Vapor-Solid (VS) model, Vapor-Liquid-Solid (VLS) model, and recently, Solution-Liquid-Solid (SLS) model. Some modifications [38] have also been published which will not be discussed here.

Vapor-Solid (VS) Model

Figure 2.5 shows an approximate growth model of vapor-solid growth mechanism. The diagram takes the growth of GaN as an example. Epitaxial growth can be achieved without catalyst or liquid phase. The sum of thermodynamic surface energy and heat of fusion become the driving force for VS growth.

Vapor-Liquid-Solid (VLS) Model

The mechanism [39] was first introduced in the 1960s to explain the growth of silicon whiskers or tubular structures [40]. In this model, growth occurs by precipitation from a supersaturated liquid-metal-alloy droplet located at the top of whisker, into which silicon atoms are preferentially absorbed from the vapor phase. The similarity between the growth of carbon nanotubes and the VLS model has also been pointed out by Saito *et al* [41][42] on the basis of their experimental findings for multi-walled nanotube growth in a purely carbon environment. Solid carbon sublimates before it melts at ambient pressure, and therefore these investigators suggested that some other disordered carbon form with high fluidity, possibly induced by ion irradiation, should replace the liquid droplet.

Solid-Liquid-Solid (SLS) Model

Figure 2.7 [43] shows diagram of solution-liquid-solid growth mechanism which takes Ⅲ-Ⅴ materials for example. No catalyst is used for solution-phase synthesis. The materials are produced as polycrystalline fibers or near-single-crystal whiskers having width of 10 to 150 nanometers and length of up to several micrometers [44]. This mechanism shows that process analogous to vapor-liquid-solid growth operated at low temperatures, while requirement of a catalyst that melts below the solvent boiling point to be its potential limitation.

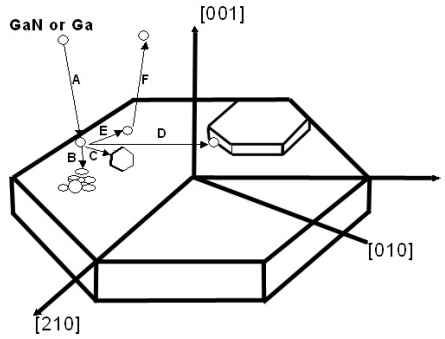

Fig. 2.5 Schematic diagram of vapor-solid (VS) growth model

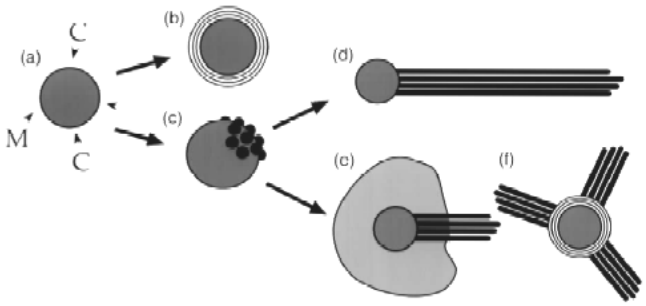

Fig. 2.6 Schematic diagram of VLS growth mechanism for nanotubes

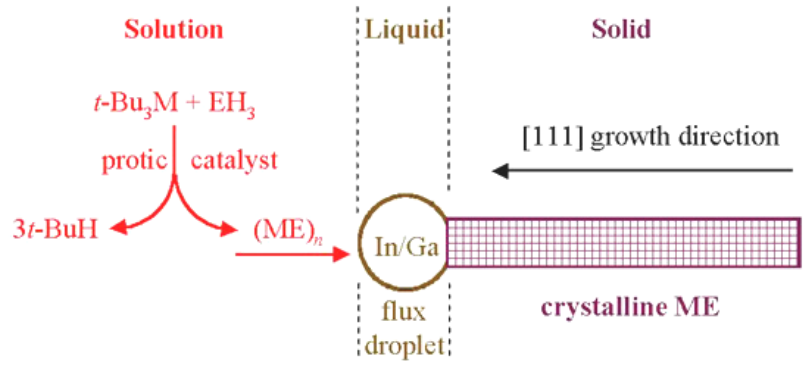

Fig. 2.7 Schematic of SLS growth mechanism

2.3 Bias Assisted Microwave Plasma Chemical Vapor Deposition

Microwave plasma chemical vapor deposition is one of the important tools for thin film deposition, micro manufacturing, and surface treatment [45]. By the advantage of high ion density, high degree of dissociation, high reactivity, and low process temperature, various of substrates are capable of fabrication under low temperature with deposition and etching, which is meaningful to LSI process, microelectronic devices, optoelectronic devices, polymers, and thin film sensors.

By applying electric field, the reaction gas breakdown to induce electrons and ions. With electromagnetic field obtained by microwave or RF power, more electrons and ions are generated by colliding with the un-dissociated gas. Stable plasma is reached when the generation rate and consumption rate are equal for all species. Unlike traditional thermal plasma, temperature of electrons, ions, and neutral particles in low temperature plasma induced by discharge are not identical. The temperature of electron is about 1000^{o}K, while the ions and neutral ones are below 500^{o}K. Therefore, low temperature plasma is a non-equilibrium plasma with not only few ions, electrons, but also excite state, transient state, and free radicals. By manipulating these high energy species, reaction which is hard for steady state species are attainable.

Taking diatomic plasma for example, the procedure may describe as follows :

(Ⅰ)Ionization

$$A_2 + e^- \rightarrow A_2^+ + 2e^-$$

(Ⅱ)Dissociative ionization

$$A_2 + e^- \rightarrow A^+ + A + 2e^-$$

(Ⅲ)Attachment

$$A_2 + e^- \rightarrow A_2^-$$

(Ⅳ)Detachment

$$A_2^- + e^- \rightarrow A_2 + 2e^-$$

(Ⅴ)Recombination

$$A_2^+ + e^- \rightarrow A_2$$

(Ⅵ)Atom recombination

$$2A^{\bullet} \rightarrow A_2$$

*any polyatomic molecule is substituent for mentioned above.

$^{\bullet}$ stands for free radical

Basically, microwave plasma chemical vapor deposition does not need any electrode or even heater. But in this thesis, bias plays an important role in the growth of nano materials, and also an essential term.

When a DC bias is added on to the substrate, before the ions pass through the plasma sheath area, the movement of the ions do not affect by the collision between the ions, comparatively and statistically. Also means the ions can strike the substrate directly and vertically by the applied field [46].